macromol

MDPI

Article

Distinct Effects of PARP1, PARP2, and PARP3 on the Structure of a Chromatin-like Particle Revealed by Atomic Force Microscopy

Alexander A. Ukraintsev, Mikhail M. Kutuzov, Ekaterina A. Belousova and Olga I. Lavrik *

Knorre Institute of Chemical Biology and Fundamental Medicine, Siberian Branch of the Russian Academy of Sciences, 8 Lavrentiev Ave., Novosibirsk 630090, Russia; alan.ukraintsev@gmail.com (A.A.U.); kutuzov.mm@mail.ru (M.M.K.); rina@1bio.ru (E.A.B.)
* Correspondence: lavrik@1bio.ru

Abstract

Compaction of chromatin and its local remodeling underlie all DNA-dependent processes in a cell. Poly(ADP-ribose)polymerases (PARP) 1, 2 and 3 are known to interact with nucleosomes, but their catalytically independent influence on the structure of nucleosomal arrays remains poorly understood. Here, using atomic force microscopy, we studied the effects of PARP1, PARP2, and PARP3 on the compaction of a chromatin-like particle, a model chromatin fragment composed of eight tandemly arranged nucleosomes. We have demonstrated here that the proteins act in distinct ways on morphometric characteristics of individual particles, namely, PARP1 loosened individual nucleosome core particles (NCP), increasing their diameter by ~18%, without changing the linker length; PARP2 did not affect the NCP scales but increased the linker length by ~60%, thereby reducing the packing density of the array; and PARP3 also left the NCPs intact but compacted the array, reducing the linker length by ~40%. Thus, the obtained results demonstrate the distinct potential of PARP-family proteins in the regulation of chromatin compaction where PARP3 may act as a factor promoting chromatin compaction at a level of the nucleosomal array.

Keywords: PARP1; PARP2; PARP3; chromatin; nucleosome; nucleosomal array; chromatin compaction; atomic force microscopy

1. Introduction

Eukaryotic genomic DNA is packaged into a nucleoprotein complex, chromatin, whose elementary structural unit is the nucleosome. The nucleosome core particle (NCP) is formed by a histone octamer (two molecules of each H2A, H2B, H3, and H4), around which 147 base-paired DNA is wrapped [1]. Adjacent NCPs are joined by linker DNA segments, forming a "beads-on-a-string" structure (~10 nm) that can further fold into more compacted higher-order organization [2,3]. The degree of chromatin compaction is not constant; it is dynamically regulated, which determines the accessibility of DNA to protein factors and thereby affects transcription, replication, and repair [2,3]. The geometry of the linker DNA plays a key role in the formation of higher-order structures: the length and orientation of the linkers substantially affect the folding of the nucleosomal fiber and its propensity for self-association [2].

The regulation of chromatin compaction is particularly important in response to DNA damage. The occurrence of a break is a trigger for local chromatin remodeling; its loosening (decompacting) provides access to repair enzymes to the lesion and then restoration of the original packing [4]. Among the earlier sensors that recognize DNA breaks and initiate such rearrangements are the DNA-dependent poly(ADP-ribose)polymerases, the PARP proteins.

Check for updates

Received: 30 September 2026
Revised: 13 November 2026
Accepted: 25 November 2026
Published: 27 November 2026

Copyright: © 2026 by the authors. Licensee MDPI, Basel, Switzerland. This article is an open access article distributed under the terms and conditions of the Creative Commons Attribution (CC BY) license.

The human PARP family comprises 17 proteins, but only 3 of them—PARP1, PARP2, and PARP3—are activated directly upon binding to DNA [5]. These enzymes covalently attach poly- (PARP1 and PARP2) or mono-(ADP-ribose) (PARP3) to target proteins using NAD^+ as a substrate. They are able to modify primarily themselves and also other proteins, including histones. The polymer serves as a signal for recruitment of the repair factors and subsequent modulation of the chromatin structure [5]. Moreover, the recent data show that catalytic activity of PARP1 and PARP2 can be modulated by supplementing their catalytic site with histone PARylation factor 1 [6–10]. Despite a common catalytic mechanism, PARP1, PARP2, and PARP3 substantially differ in both domain architecture and function [5].

PARP1 is the most abundant nuclear member of the family and the most extensively studied. The majority of cellular poly(ADP-ribosyl)ation is produced by PARP1 [5]. In addition to its key role in repair, PARP1 is directly involved in the regulation of chromatin structure and transcription [11–17]. Upon activation in response to DNA damage, poly(ADP-ribosyl)ation of histones and of PARP1 itself promotes the recruitment of the PAR-dependent remodeler ALC1/CHD1L, chromatin loosening, and attraction of the DNA repair machine [4]. Moreover, single-molecule FRET experiments had shown that PARP1 itself is able to partially unwind nucleosomal DNA, increasing the distance between adjacent DNA gyres without loss of histones [18]. On the other hand, unmodified PARP1 binds the nucleosome in a histone-H1-like manner, competing with the linker histone H1 at the dyad region that promotes nucleosome juxtaposition and the compaction of nucleosomal arrays [11,12]. Thus, the interaction of PARP1 with chromatin can potentially lead to opposite context-dependent effects [13,19].

PARP2 partially duplicates the functions of PARP1 in the DNA-damage response and exhibits a higher affinity for the nucleosome than for free DNA [14]. According to the structural data, PARP2 is able to recognize DNA breaks [20] and to form a bridge between two nucleosomes, fitting tightly the DNA ends at a double-strand break [21,22].

PARP3 is specialized in the recognition of single-strand breaks, including those in the nucleosomal context. Upon binding to a nick-containing nucleosome, it mono(ADP-ribosyl)ates histone H2B at the Glu2 residue [23]. Additionally, we have previously shown by atomic force microscopy (AFM) that PARP3 alters nucleosome geometry towards compaction [24].

Despite considerable progress in understanding the interaction of PARP proteins with individual nucleosomes [24,25], the influence of these proteins on the structure of extended nucleosomal arrays remains poorly understood and has been characterized predominantly for PARP1 to date only [11,12]. Meanwhile, the effects that cannot be observed using mononucleosome substrates may become apparent specifically at the level of the nucleosomal array at the formation of contacts between nucleosomes or the DNA looping. The effect of a protein at both organization levels at the structure of the individual core particle and the array package can be detected by methods that provide single-molecule resolution. AFM is one such method; it makes it possible to visualize individual molecules of nucleoprotein complexes under near-native conditions and to characterize their geometry quantitatively, which makes it an effective tool for studying chromatin structure [26].

In the present work, the effects of the DNA-dependent proteins PARP1, PARP2, and PARP3 on the structure of a model chromatin fragment, a chromatin-like particle (CLP), have been investigated by AFM. The CLPs were composed of eight nucleosomes assembled on the nucleosome-positioning sequence Widom clone 601 [27] interspersed with 25 bp linkers and carried reference DNA tails [28]. The combination of population analysis, which includes estimating of molecule projection area and the volume, along with morphometric analysis of individual particles—specifically measuring the diameters of individual NCPs, their circumscribed circle radius, and center-to-center length—enabled the separation of

each protein's effects on levels of compaction. This analysis suggests a role for nuclear PARP proteins in the regulation of chromatin rearrangement, a step that can be separated from the ADP-ribose transferase activity.

2. Materials and Methods

2.1. Reagents and Equipment

The following reagents and materials were used: 3.5 kDa dialysis membranes (Spectrum Laboratories Inc., Rancho Dominguez, CA, USA); bromophenol blue (Fluka, Buchs, Switzerland). Most of the reagents used in the study were purchased from Sigma (St. Louis, MO, USA). To produce the target CLP 601-8 DNA, the 8 × 601-pKYB1 plasmid, containing the corresponding 8 × nucleosome-positioning sequence Widom clone 601 inserts [29], was used. Recombinant Taq DNA polymerase was kindly provided by S. N. Khodyreva (Knorre Institute of Chemical Biology and Fundamental Medicine, Siberian Branch of the Russian Academy of Sciences (ICBFM SB RAS), Novosibirsk, Russia). The recombinant proteins—human PARP1, mouse PARP2, human PARP3, and histone octamers of H2A, H2B, H3, and H4 from *Gallus gallus*—were produced and purified as described in [30–32]. AFM imaging was performed on a Multimode 8 instrument (Bruker, Billerica, MA, USA) using NSG01_DLC probes (TipsNano, Tallinn, Estonia). The amplicon was recovered from the agarose gel using the CleanUp Standard kit (Evrogen, Moscow, Russia).

2.2. Amplification of the CLP DNA

The DNA-containing substrate used in the experiments was obtained by PCR from the 8-nucleosome "Clone 601" plasmid vector using unique primers. The DNA construct contains eight tandem repeats of the 147 bp Widom 601 clone DNA sequence, separated from one another by 25 bp linker DNA regions. The repeats are flanked by plasmid DNA sequences of 450 and 200 bp. The primer oligonucleotides 5′-ACCGGGTTGGACTCAAGACGATAGTTACCGGATAA-3′ and 5′-CTTAACTATGCGGCATCAGAGCAGATTGTACTGAG-3′ were synthesized at the Laboratory of Biomedical Chemistry, ICBFM SB RAS (Novosibirsk, Russia). The following PCR program was used: 3 min at 95 °C; 30 cycles of 20 s at 94 °C, 20 s at 73.3 °C, and 3 min at 72 °C; with a final step of 3 min at 72 °C. After PCR synthesis, the DNA substrate was purified by agarose gel electrophoresis and recovered from the gel using the commercially available CleanUp Standard kit according to the manufacturer's instructions.

2.3. CLP Assembly

The CLP assembly was carried out according to a protocol we described previously [33], with minor modifications. A reaction mixture (100 µL) containing 20 nM CLP DNA and 160 nM histone octamers (molar ratio 1:8, i.e., one octamer per nucleosome-positioning sequence) in buffer (0.2 mM EDTA, 1.6 mM CHAPS, 10 mM Tris-HCl, pH 7.5, and 5 mM β-mercaptoethanol) was mixed with 2M NaCl followed by dialysis with a gradient of NaCl concentration to a final concentration of 10 mM NaCl overnight at room temperature. The quality of the assembly was assessed by AFM.

2.4. Preparation of the CLPs and Their Complexes with PARP1, PARP2 and PARP3 for AFM Scanning

For studying CLPs and their complexes with PARP proteins by AFM, immobilization on the freshly cleaved mica surface with nickel (II) chloride ($NiCl_2$) was used [34,35]. The reaction mixture consisted of 10 nM CLP601-8, buffer (20 mM NaCl, 0.2 mM EDTA, 1.6 mM CHAPS, 10 mM Tris-HCl, pH 7.5, and 5 mM β-mercaptoethanol), and one of the PARPs at a concentration of 66 nM. This PARP concentration was chosen as sufficient for the binding of most of the CLPs but not causing aggregation of the sample on the AFM images. The reaction mixture was incubated for 15 min at 37 °C. The samples were then

diluted 10-fold with 10 mM HEPES (pH = 8.0) supplemented with 5 mM $NiCl_2$, giving a final CLP concentration of 1 nM, which provides a uniform distribution of the particles over the surface with little or no crowding, and immediately applied to the mica surface. After application, the mica surface was washed three times with 1 mL of Milli-Q water and dried under a gentle stream of argon. Prior to imaging, the samples were stored in a desiccator over solid NaOH.

Control samples containing free PARP1, PARP2, or PARP3 proteins, immobilized on a mica surface using NiCl2, are presented in the Supplementary Materials (Figures S1–S3).

2.5. AFM Scanning

Scanning was performed on a Multimode 8 instrument (Bruker, Billerica, MA, USA) in tapping mode (TappingMode) in air. Carbon cantilevers NSG01_DLC (TipsNano, Tallinn, Estonia) with a tip resonance frequency of 90–180 kHz were used for scanning. A typical acquired image was 2 μm × 2 μm at 1024 pixels per line. The scan rate was 0.5 Hz.

2.6. Processing of the AFM Images

All samples were prepared in parallel from the same CLP preparation, deposited on mica in the same way, and imaged in one session with the same probe. Images of the CLP were collected from 12, the CLP supplemented with PARP2 and PARP3 from 10, and the CLP supplemented with PARP1 from 8 non-overlapping areas of the mica surface. The control AFM images with PARP1, PARP2 and PARP3 are shown in Supplementary Materials.

At first, all images were processed in Gwyddion v.2.65 (http://gwyddion.net/, accessed on 19 July 2026). CLPs were detected with the "Grain finding" tool using a height threshold of 0.5 nm above the background, which excludes naked DNA from the CLP mask (Figure S4). Individual pixels or regions on the DNA higher than 0.5 nm were additionally removed manually, without affecting the NCP region. For each CLP the projection area of the mask onto the plane (S) and the volume between the surface and the Laplace-interpolated background (V) were measured. The projection area of the CLP is the sum of the areas of individual NCPs. The radius (R) of the circle, which was circumscribed around the outermost NCPs (with naked DNA excluded), was obtained with the "Grain measurement" tool.

The diameter (d) and height (h) of individual NCPs were determined from the cross-section profiles of each NCP (Gwyddion "Profile" tool): d as the full width at half of a profile maximum and h as the profile height (Figure S5). The center-to-center distance between adjacent NCPs was measured as a distance of the heights' maxima. The apparent linker length (l) was measured in ImageJ v.1.53e (https://imagej.nih.gov/ij/, accessed on 19 July 2026) as the projected length of DNA between the edges of two adjacent NCP discs (defined by the half-maximum boundaries), traced along the DNA path. The lengths of DNA tails T1 and T2 were measured from the DNA end to its entry point into the terminal NCP discs. The expected contour lengths of T1 and T2 are 153 and 68 nm.

For the morphometric analysis, four CLPs per sample were selected according to (i) lying within the mode of the S–V distribution of the respective population (Figure S6; ranges are given in Section 3), (ii) containing eight NCPs, and (iii) having both DNA tails resolved unambiguously. The selected particles are shown in Figure S7. This gives 32 NCPs and 28 linkers, 4 T1s, and 4 T2s to analysis.

Parameters measured for the whole particles from the population (S, V, and R) were compared using the Mann–Whitney test with the Bonferroni correction in three comparisons with ±SD. The sample volumes are N = 98 for the control CLP, 96 for the CLP supplemented with PARP1, and 100 with PARP2 or PARP3 (Figures S6 and S8). Morphometric parameters (d, l, center-to-center distance, T1, and T2) were compared using Student's t-test with 95% of

confidence as indicated in the figure legends. Data were analyzed and plotted in Microsoft Excel 2016.

3. Results and Discussion

The details of the interaction of PARP1, PARP2, and PARP3 proteins with chromatin have been a subject of the present study. This study was undertaken to understand the possible interaction of nuclear PARP proteins with nucleosome or chromatin fragment that processed independently on PARP activation and the following NAD^+ dependent synthesis of polymer. For this reason, we used a construct containing a tandem of eight nucleosomes, CLP, as a model of a chromatin fragment. It is known that the length of linker DNA in chromatin can vary over a wide range, with a minimum of about 20 bp [3]. In this work the linker is 25 bp. The DNA tails were 450 and 200 bp long and have served as reference markers that made it possible to identify the individual NCPs. The CLPs were assembled by salt-gradient dialysis from the corresponding dsDNA and octamers of the core histones H2A, H2B, H3, and H4, isolated from *Gallus gallus* erythrocytes. The broad range of potential PTMs on histones and their variants derived from a natural source makes this model heterogeneous but allows it to suggest it as a common model of different chromatin forms.

CLP assembly has been approved by AFM. Figure 1 shows a typical AFM image of a single CLP that displayed the expected "beads-on-a-string" morphology [3] and contained eight individual NCPs. The raw CLPs images are provided in Figure S9.

The geometric parameters of the individual NCPs have been matched with the expected values, indicating the correct CLP assembly. Definitely, the average NCPs diameter and height were 13 nm and 2.6 nm, respectively [36]. The lengths of the tails of DNA corresponded to the theoretical values that indicate correct positioning of NCPs on the DNA molecule during CLP reconstitution (T1: 140 nm vs. 153 nm; T2: 65 nm vs. 68 nm, respectively; Figure 1). The distribution of the CLPs by the number of NCPs per molecule is shown in Figure 2.

The mean number of NCPs per CLP was 7.3, and the most abundant class contained 8 NCPs. Thus, the obtained CLP substrate is a model of a nucleosomal array.

Next, we examined the changes in the CLP parameters in the presence of PARP proteins. To this end, the CLP samples were supplemented with PARPs before AFM analysis. The biochemical parameters of the complexes of NCP/PARPs are well characterized up to date. The concentrations of the components for AFM experiments were in accordance with the corresponding dissociation constants of the NCP/PARPs complexes. The CLP/PARP complexes have been visualized by AFM (Figures S10–S12) and measured in the same way as the control CLPs. The measured projection areas (S) and volumes (V) are presented in Figure 3.

The presence of any of the three proteins provided a significant increase in both the volume and the projection area relative to the control. The observed effects could be attributed either to the presence of bound proteins or to CLP transformations caused by the PARPs. We did not make any fixation to stabilize the composition of the complex; thus, CLP/PARP complexes are expected to dissociate to a large extent during the washing of the mica. It should be noted that AFM allows visualization of the intermediate state of a system during immobilization on mica due to kinetic trapping [37,38]. Taking it into account, we assumed that CLP retains the state that occurred in the solution.

As can be seen from Figure 3, PARPs influenced the projection area and the volume differently. Complexes of PARP1 with CLP showed the largest means of the values of area and volume; complexes of PARP2, the smallest mean of the value of projection area; and complexes of PARP3, the smallest mean of the values of volume. These obser-

vations suggest that modes of different PARP binding to the NCP result in distinct CLP conformations [11,12,14,20–24]. At the same time, alternative interactions of the PARPs with the nucleosomal array cannot be ruled out.

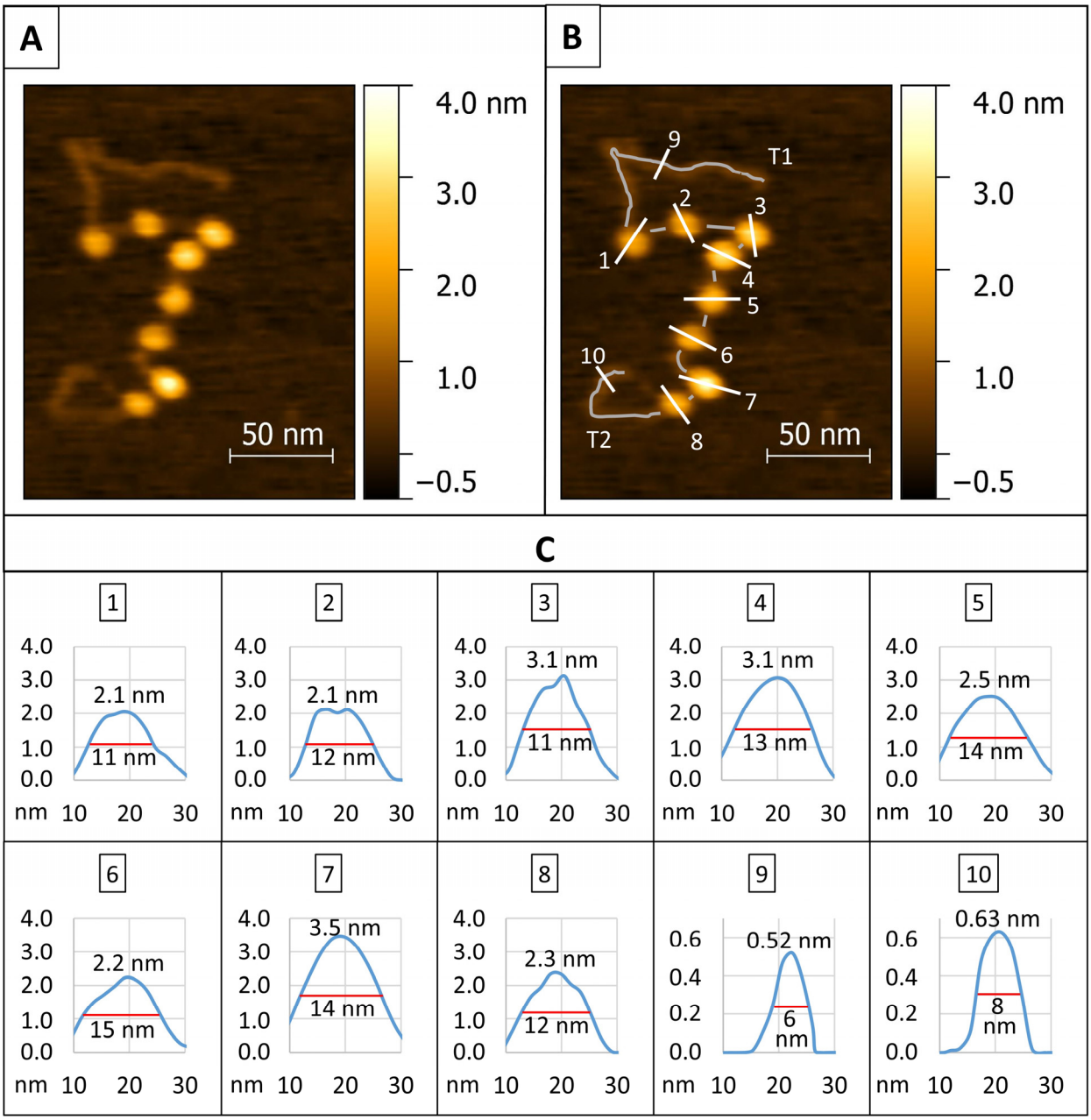


Figure 1. The measurement method of CLP. (**A**) Typical AFM image of a CLP. Each bright spot corresponds to an individual NCP. (**B**) The positions of the sections (white lines) used for the measurement of the 2D profiles. Points 1–8 in B within a CLP are NCPs. Points 9 and 10 are dsDNA regions. Grey lines indicate the contour of the dsDNA. (**C**) The corresponding 2D profiles. The height and the width at half-maximum are indicated for each measurement. For profiles 1–8, the height scale ranges from 0 to 4 nm, while, for profiles 9 and 10, it ranges from 0 to 0.6 nm.

To this end, we plotted V against S for all the measured complexes in order to select the most representative molecules for further analysis (Figure S6). The corresponding projection area and volume values were 1500–1750 nm^2 and 2000–2800 nm^3 for the control CLP; 2250–2500 nm^2 and 3600–4200 nm^3 for the CLP/PARP1 complexes; 2000–2400 nm^2 and 3600–4000 nm^3 for the CLP/PARP2 complexes; and 1900–2300 nm^2 and 2800–3200 nm^3 for

the CLP/PARP3 complexes. According to these parameters, we selected four AFM images of individual CLPs for each sample type that contained eight nucleosomes and both DNA tails resolved unambiguously (Figure S7). The typical images are shown in Figure 4.

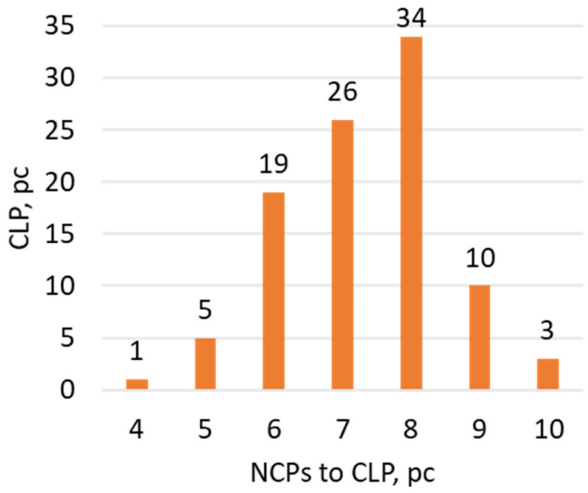


Figure 2. Distribution of the number of NCPs per CLP molecule ($N = 98$).

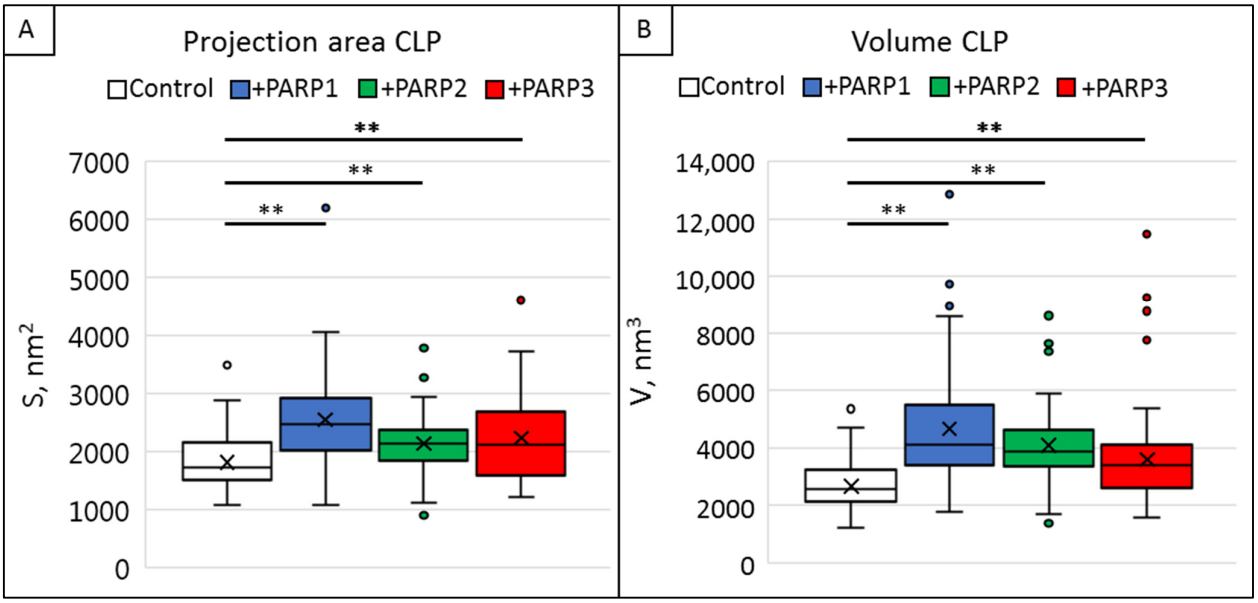


Figure 3. Projection area (**A**) and volume (**B**) of the CLP complexes. Box plots for the control (white boxes) and for the samples supplemented with PARP1 (blue boxes), PARP2 (green boxes), and PARP3 (red boxes). Mean values of S and V. Asterisks indicate statistically significant differences from the control: ** $p \leq 0.01$. For each sample the number of CLP was at least 96. For parameters measured for the whole particles, see Section 2.6.

The lengths of the tails lay in the range of 150 nm for T1 and 64 nm for T2, close to the contour lengths expected for 450 and 200 bp, respectively (Figure 5). Student's t-test revealed no significant differences between the samples ($p > 0.05$). This confirms that the NCPs were assembled on the nucleosome-positioning sequences. Therefore, the differences in the morphometric parameters between the samples arise within the nucleosomal part of the construct.

The projection area and volume are integral characteristics of the CLP, and formally the same increment value can be produced by two structurally uncommon events. The CLP is a set of NCPs interspaced by linker DNA. On the one hand, if an NCP is approximated

by a disc of diameter d and effective height h, its projection area is proportional to d^2 and the volume is proportional to d^2h. Both quantities are proportional to d^2, so that even a moderate loosening of the core—a partial unwrapping of the outer DNA turn that increases d by ~10%—would give ~20% more projection area and volume per NCP and, summed over eight NCPs, a measurable increment. On the other hand, the relative position of the NCPs can also influence the projection area and the volume. Therefore, we additionally analyzed the linker length, l, measured between the projections of two adjacent nucleosomal discs along the DNA track, which may reflect dynamic changes of the entire CLP (Figure 6A). To determine the contour length of the linker DNA accurately, the measurements were taken along the DNA strand, as shown in Figure 1B (grey lines).

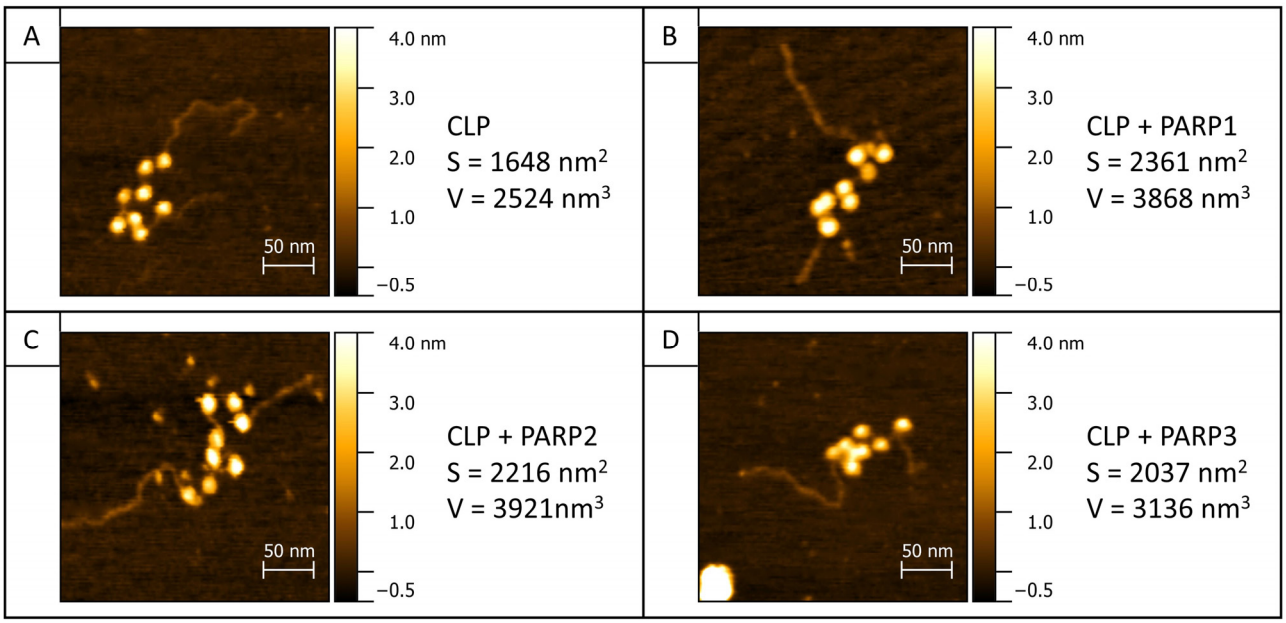


Figure 4. Representative AFM images of individual CLPs assembled in the absence (**A**) or in the presence of PARP1 (**B**), PARP2 (**C**), and PARP3 (**D**).

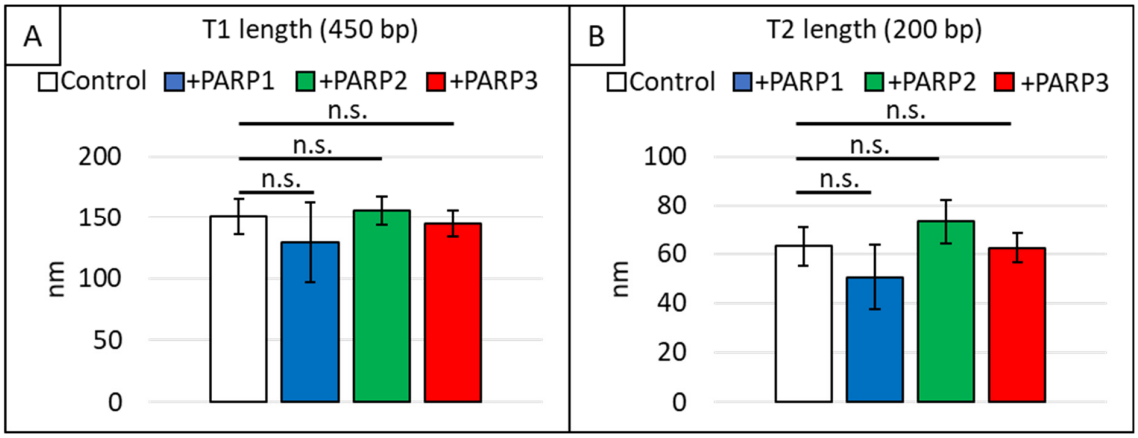
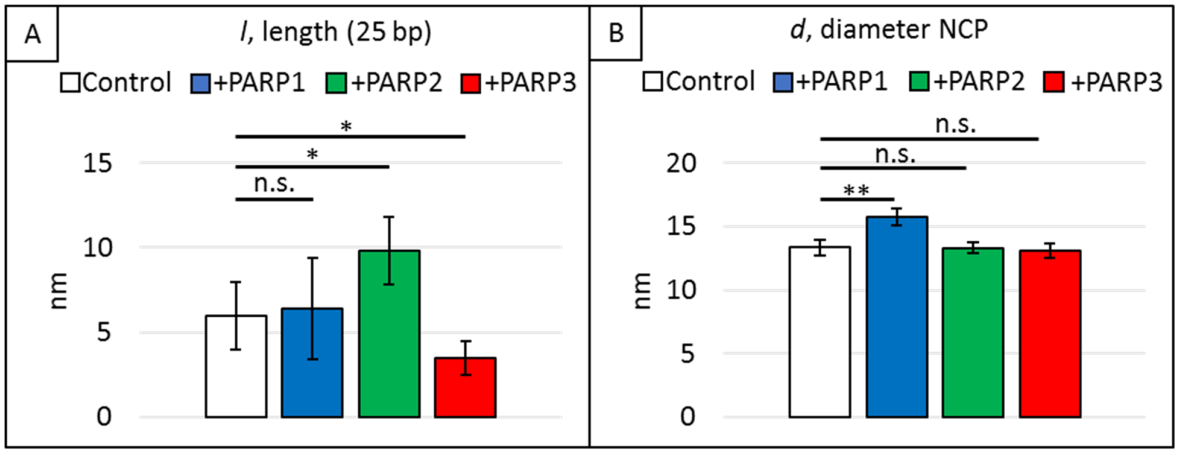


Figure 5. Bar charts of the DNA tails 1 ((**A**), T1) and 2 ((**B**), T2) lengths measured on the four selected molecules of each sample. White is for CLP; blue is for CLP+PARP1; green is for CLP+PARP2; and red is for CLP+PARP3. Bar height is the mean DNA tail length (nm); error bars reflected ±SD. n.s. is not significant. For the morphometric analysis, see Section 2.6.

We previously showed that PARP binding can alter the geometry of the NCP, as reflected by the opening angle between the entering and exiting DNA arms [24]. Additionally, we measured the diameter of the individual NCPs, d (Figure 6B).



	Control	+PARP1	+PARP2	+PARP3
l, nm	6.0 ± 2.1	6.4 ± 3.0	9.8 ± 2.6	3.5 ± 1.4
d, nm	13.4 ± 0.6	15.8 ± 0.6	13.3 ± 0.4	13.1 ± 0.6

Figure 6. (**A**) Bar charts of the linker length, *l*, obtained from the analysis of four CLPs in each group. (**B**) Bar chart of the diameter of the individual NCPs, *d*, obtained from the analysis of four CLPs in each group. White is for CLP; blue is for CLP+PARP1; green is for CLP+PARP2; and red is for CLP+PARP3. Bar height is the mean value (nm); error bars are 95% confidence intervals calculated by Student's *t*-test. n.s. is not significant; * $p < 0.05$; ** $p < 0.01$. The values of the parameters shown in the charts are presented in the table. For the morphometric analysis, see Section 2.6.

As can be seen in Figure 6, both values corresponded to the expected ones in the control sample (Figure 6A,B, white bars). Misassembly of an NCP or skipping of a nucleosome-positioning sequence would extend the apparent linker. The uniform values of *l* observed, therefore, provide evidence that the selected CLPs are correctly assembled from eight NCPs and could serve as the reference point for the analysis of the complexes.

In the presence of PARP1, *l* was not changed significantly ($p > 0.05$), whereas *d* was increased by ~18% ($p < 0.01$); that is consistent with the largest values of *S* and *V* obtained for this complex, since both are proportional to d^2 (Figure 6A,B, blue bars). It could imply packing invariation in combination with an individual NCP loosening. This output is consistent with the single-particle FRET data showing that PARP1 binding leads to an increase in the distance between adjacent gyres of nucleosomal DNA, i.e., to reversibly partially nucleosomal DNA uncoiling without apparent loss of histones [18,39]. Alongside that, the AFM study had not indicated any significant changes in opening angle between prolonged DNA arms of NCP under PARP1 binding that could potentially suggest the absence or minor influence of PARP1 to CLP compaction changing [24].

At first sight, these data are at odds with the obtained ability of PARP1 to promote chromatin compaction [11,12]. However, the discrepancy can be explained by the properties of the systems applied. The authors of [12] studied the impact of PARP1 on compaction by AFM using a plasmid carrying several tens of physiologically spaced nucleosomes reconstituted with native *Drosophila* core histones that were stabilized with glutaraldehyde before deposition on mica. It can be supposed that the condensation had been attributed to the bridging of distant DNA segments by PARP1 and DNA loop stabilization [40,41]. Both the number of nucleosomes and the persistence length of the DNA composing the CLP make such contacts remote. In addition, chemical treatment fixes a single spatial complex

conformation, whereas in its absence we received a set of conformations of PARP-compacted CLP upon deposition on mica. The advantage of the last approach is the possibility of obtaining any changes at the individual NCP level upon PARP1 binding. The loosening of NCP observed upon PARP1 binding is in line with its cellular functions that do not relate to DNA repair but are expected to directly involve it in transcription regulation and the maintenance of a chromatin permissive state [11,13,19,39].

The presence of PARP2 led to the opposite PARP1 parameter pattern: the *d* of individual NCPs remained at the control level ($p > 0.05$), while *l* increased by ~60% ($p < 0.05$) (Figure 6A,B, green bars). This fact indicates the absence of changes at the level of the individual NCPs with a pronounced loosening of the entire CLP structure. PARP2 is able to engage the DNA breaks to bridge two independent NCPs [20,21,42]. On the other part, PARP2 does not co-condense with dsDNA, in contrast to PARP1 [43], and therefore lacks the alternative, condensation-based route to juxtaposing distant DNA segments. Additionally, based on published data, it can be proposed that the interaction of PARP2 with NCP could be mediated not only by DNA binding but also by the histones and occur outside of the entry–exit region, since PARP2 does not influence the compaction degree of an NCP with extended DNA arms [14,24]. Here the CLP contains the undamaged DNA, so the interaction is limited by the core. Thus, the major consequence of PARP2 binding was not the juxtaposition of neighboring NCPs but a moderate decrease in the packing density of the NCP array.

The presence of PARP3 did not trigger changes in the core ($p > 0.05$) but led to a shortening of *l* by ~42% ($p < 0.05$), that is, compaction of the CLP (Figure 6A,B, red bars). This result correlates with the previously observed one in the study of the PARP3 interaction with an NCP containing extended DNA arms and transmits the role of the protein in maintaining the next level of compaction organization [24]. In vitro experiments have indicated that PARP3 binds the nucleosome rather than naked DNA [25]. In the cell, PARP3 has been found in association with polycomb group proteins [44], which are a part of a system responsible for the maintenance of transcriptionally silent, compacted chromatin. Overall, PARP3 could provide a higher compaction level, which does not require any alteration of the nucleosomal core but is realized at the level of the nucleosomal array (Figure S8). Analysis of the entire population of particles showed that the radius of the circle circumscribing the NCPs most distant from the center is decreased significantly only in the presence of PARP3; this fact confirms the conclusion drawn, independently of the single-molecule measurement results (Figure S8).

4. Conclusions

In the present work, AFM was used to compare the effects of the three DNA-dependent poly(ADP-ribose)polymerases, PARP1, PARP2, and PARP3, on a chromatin-like particle assembled from eight tandem nucleosomes. It was found that the presence of any of the three proteins resulted in a significant increase in the projection area and the volume of the CLP. However, this integral response resulted from distinct interaction modes at two independent levels of organization, that is, individual core particle and common CLP package. PARP1 loosened the individual NCPs without rearranging the CLP packing. PARP2 does not influence the core particle but has loosened the CLP. PARP3 has also left the core intact but has provided substantial compaction of the CLP. Of the three proteins, PARP3 alone may therefore provide a compacting function on nucleosome-covered DNA without implication in the core particle. Together with the previously reported data concerning the cellular localization and interaction with NCP, these argue for a potential specific architectural role of the processes maintaining chromatin compaction.

It should be noted that this study contains certain assumptions that were necessary to examine the direct effect of PARP proteins on CLP structure under protein binding. It precluded an assessment of the impact of PARylation. Furthermore, extrapolating these results to cellular conditions would require the use of more complex and extended chromatin arrays including linker histone H1, which promotes chromatin compaction, as well as antagonizing non-histone chromatin proteins.

Supplementary Materials: The following supporting information can be downloaded at: https://www.mdpi.com/article/10.3390/macromol6040119/s1. Figure S1: Overview AFM image of PARP1. Figure S2: Overview AFM image of PARP2. Figure S3: Overview AFM image of PARP3. Figure S4: Processing of chromatin-like particle (CLP) AFM images by height-threshold masking for the measurement of the projection area (S), volume (V) and radius of the circle circumscribed around the nucleosome core particles (NCPs). Figure S5: Bar charts of the centre-to-centre NCP linker length (L) and the height of individual NCPs (h) for CLP and for CLP supplemented with PARP1, PARP2 or PARP3 (four molecules per group; mean with 95% confidence interval). Figure S6: Distribution of the volume against the projection area of individual particles, with marginal frequency histograms (N = 98 for CLP, 96 for CLP/PARP1, 100 for CLP/PARP2 and 100 for CLP/PARP3). Figure S7: AFM images of four individual CLPs assembled alone and in the presence of PARP1, PARP2 and PARP3. Figure S8: Radius R of the circle circumscribed around the outermost nucleosomes, with the terminal DNA tails excluded, for CLP and for the CLP/PARP1, CLP/PARP2 and CLP/PARP3 samples (mean with 95% confidence interval). Figure S9: Overview AFM image of the control CLP preparation. Figure S10: Overview AFM image of the CLP/PARP1 complexes. Figure S11: Overview AFM image of the CLP/PARP2 complexes. Figure S12: Overview AFM image of the CLP/PARP3 complexes.

Author Contributions: Conceptualization, A.A.U., M.M.K. and O.I.L.; methodology, A.A.U. and M.M.K.; investigation, A.A.U.; resources, E.A.B. and M.M.K.; formal analysis, A.A.U.; visualization, A.A.U.; writing—original draft preparation, A.A.U.; writing—review and editing, M.M.K., E.A.B. and O.I.L.; supervision, O.I.L.; project administration, O.I.L.; funding acquisition, O.I.L. All authors have read and agreed to the published version of the manuscript.

Funding: This work was supported by the state assignment for ICBFM SB RAS No. 125012300658-9 (production and purification of PARP2 protein) and by Russian Science Foundation grants No. 25-74-30006 (production and purification of PARP1 protein) and No. 21-64-00017П (production and purification of PARP3 protein, preparation of nucleosomes, biochemical experiments, and AFM experiments).

Institutional Review Board Statement: Not applicable.

Informed Consent Statement: Not applicable.

Data Availability Statement: The data presented in this study are available on request from the corresponding author. The raw AFM images and the primary morphometric measurements are not publicly archived owing to their size. The original data presented in the study are openly available at https://drive.google.com/file/d/1G47JDh5AZq1flUdskiNQdjzlLTpfaifx/view?usp=drive_link (accessed on 24 November 2026).

Acknowledgments: The authors thank M. A. Khodorkovskii (Peter the Great St. Petersburg Polytechnic University, Russia) for the 8 × 601-pKYB1 plasmid and S. N. Khodyreva (ICBFM SB RAS) for the recombinant Taq DNA polymerase.

Conflicts of Interest: The authors declare no conflicts of interest.

Abbreviations

The following abbreviations are used in this manuscript:

AFM	Atomic Force Microscopy
CLP	Chromatin-Like Particle
NCP	Nucleosome Core Particle
PARP	Poly(ADP-ribose)Polymerase

References

1. Luger, K.; Mäder, A.W.; Richmond, R.K.; Sargent, D.F.; Richmond, T.J. Crystal structure of the nucleosome core particle at 2.8 Å resolution. *Nature* **1997**, *389*, 251–260. [CrossRef]
2. Grigoryev, S.A. Chromatin higher-order folding: A perspective with linker DNA angles. *Biophys. J.* **2018**, *114*, 2290–2297. [CrossRef]
3. Szerlong, H.J.; Hansen, J.C. Nucleosome distribution and linker DNA: Connecting nuclear function to dynamic chromatin structure. *Biochem. Cell Biol.* **2011**, *89*, 24–34. [CrossRef]
4. Sellou, H.; Lebeaupin, T.; Chapuis, C.; Smith, R.; Hegele, A.; Singh, H.R.; Kozlowski, M.; Bultmann, S.; Ladurner, A.G.; Timinszky, G.; et al. The poly(ADP-ribose)-dependent chromatin remodeler Alc1 induces local chromatin relaxation upon DNA damage. *Mol. Biol. Cell* **2016**, *27*, 3791–3799. [CrossRef]
5. van Beek, L.; McClay, É.; Patel, S.; Schimpl, M.; Spagnolo, L.; Maia de Oliveira, T. PARP power: A structural perspective on PARP1, PARP2, and PARP3 in DNA damage repair and nucleosome remodelling. *Int. J. Mol. Sci.* **2021**, *22*, 5112. [CrossRef]
6. Gibbs-Seymour, I.; Fontana, P.; Rack, J.G.M.; Ahel, I. HPF1/C4orf27 is a PARP-1-interacting protein that regulates PARP-1 ADP-ribosylation activity. *Mol. Cell* **2016**, *62*, 432–442. [CrossRef]
7. Suskiewicz, M.J.; Zobel, F.; Ogden, T.E.H.; Fontana, P.; Ariza, A.; Yang, J.C.; Zhu, K.; Bracken, L.; Hawthorne, W.J.; Ahel, D.; et al. HPF1 completes the PARP active site for DNA damage-induced ADP-ribosylation. *Nature* **2020**, *579*, 598–602. [CrossRef]
8. Bonfiglio, J.J.; Fontana, P.; Zhang, Q.; Colby, T.; Gibbs-Seymour, I.; Atanassov, I.; Bartlett, E.; Zaja, R.; Ahel, I.; Matic, I. Serine ADP-ribosylation depends on HPF1. *Mol. Cell* **2017**, *65*, 932–940. [CrossRef]
9. Kurgina, T.A.; Moor, N.A.; Kutuzov, M.M.; Naumenko, K.N.; Ukraintsev, A.A.; Lavrik, O.I. Dual function of HPF1 in the modulation of PARP1 and PARP2 activities. *Commun. Biol.* **2021**, *4*, 1259. [CrossRef]
10. Kurgina, T.A.; Moor, N.A.; Kutuzov, M.M.; Endutkin, A.V.; Lavrik, O.I. Deciphering the dark side of histone ADP-ribosylation: What structural features of damaged nucleosome regulate the activities of PARP1 and PARP2. *Nucleic Acids Res.* **2025**, *53*, gkaf864. [CrossRef]
11. Kim, M.Y.; Mauro, S.; Gévry, N.; Lis, J.T.; Kraus, W.L. NAD+-dependent modulation of chromatin structure and transcription by nucleosome binding properties of PARP-1. *Cell* **2004**, *119*, 803–814. [CrossRef]
12. Wacker, D.A.; Ruhl, D.D.; Balagamwala, E.H.; Hope, K.M.; Zhang, T.; Kraus, W.L. The DNA binding and catalytic domains of poly(ADP-ribose) polymerase 1 cooperate in the regulation of chromatin structure and transcription. *Mol. Cell. Biol.* **2007**, *27*, 7475–7485. [CrossRef]
13. Kraus, W.L. Transcriptional control by PARP-1: Chromatin modulation, enhancer-binding, coregulation, and insulation. *Curr. Opin. Cell Biol.* **2008**, *20*, 294–302. [CrossRef]
14. Kutuzov, M.M.; Belousova, E.A.; Kurgina, T.A.; Ukraintsev, A.A.; Vasil'eva, I.A.; Khodyreva, S.N.; Lavrik, O.I. The contribution of PARP1, PARP2 and poly(ADP-ribosyl)ation to base excision repair in the nucleosomal context. *Sci. Rep.* **2021**, *11*, 4849. [CrossRef]
15. Kutuzov, M.M.; Sayfullina, D.; Belousova, E.A.; Lavrik, O.I. HPF1 regulates Pol β efficiency in nucleosomes via the modulation of total poly(ADP-ribose) synthesis. *Int. J. Mol. Sci.* **2025**, *26*, 1794. [CrossRef]
16. Smith, R.; Zentout, S.; Rother, M.; Bigot, N.; Chapuis, C.; Mihuț, A.; Zobel, F.F.; Ahel, I.; van Attikum, H.; Timinszky, G.; et al. HPF1-dependent histone ADP-ribosylation triggers chromatin relaxation to promote the recruitment of repair factors at sites of DNA damage. *Nat. Struct. Mol. Biol.* **2023**, *30*, 678–691. [CrossRef]
17. Nosella, M.L.; Kim, T.H.; Huang, S.K.; Harkness, R.W.; Goncalves, M.; Pan, A.; Tereshchenko, M.; Vahidi, S.; Rubinstein, J.L.; Lee, H.O.; et al. Poly(ADP-ribosyl)ation enhances nucleosome dynamics and organizes DNA damage repair components within biomolecular condensates. *Mol. Cell* **2024**, *84*, 429–446.e17. [CrossRef]
18. Sultanov, D.C.; Gerasimova, N.S.; Kudryashova, K.S.; Maluchenko, N.V.; Kotova, E.Y.; Langelier, M.F.; Pascal, J.M.; Kirpichnikov, M.P.; Feofanov, A.V.; Studitsky, V.M. Unfolding of core nucleosomes by PARP-1 revealed by spFRET microscopy. *AIMS Genet.* **2017**, *4*, 21–31. [CrossRef]
19. Sobotka, A.A.; Tempera, I. PARP1 as an epigenetic modulator: Implications for the regulation of host-viral dynamics. *Pathogens* **2024**, *13*, 131. [CrossRef]
20. Obaji, E.; Haikarainen, T.; Lehtiö, L. Structural basis for DNA break recognition by ARTD2/PARP2. *Nucleic Acids Res.* **2018**, *46*, 12154–12165. [CrossRef]
21. Gaullier, G.; Roberts, G.; Muthurajan, U.M.; Bowerman, S.; Rudolph, J.; Mahadevan, J.; Jha, A.; Rae, P.S.; Luger, K. Bridging of nucleosome-proximal DNA double-strand breaks by PARP2 enhances its interaction with HPF1. *PLoS ONE* **2020**, *15*, e0240932. [CrossRef]
22. Bilokapic, S.; Suskiewicz, M.J.; Ahel, I.; Halic, M. Bridging of DNA breaks activates PARP2-HPF1 to modify chromatin. *Nature* **2020**, *585*, 609–613. [CrossRef]
23. Grundy, G.J.; Polo, L.M.; Zeng, Z.; Rulten, S.L.; Hoch, N.C.; Paomephan, P.; Xu, Y.; Sweet, S.M.; Thorne, A.W.; Oliver, A.W.; et al. PARP3 is a sensor of nicked nucleosomes and monoribosylates histone H2B(Glu2). *Nat. Commun.* **2016**, *7*, 12404. [CrossRef]

24. Ukraintsev, A.; Kutuzov, M.; Belousova, E.; Joyeau, M.; Golyshev, V.; Lomzov, A.; Lavrik, O. PARP3 affects nucleosome compaction regulation. *Int. J. Mol. Sci.* **2023**, *24*, 9042. [CrossRef]
25. Ukraintsev, A.A.; Belousova, E.A.; Kutuzov, M.M.; Lavrik, O.I. Study of interaction of the PARP family DNA-dependent proteins with nucleosomes containing DNA intermediates of the initial stages of BER process. *Biochemistry* **2022**, *87*, 331–345. [CrossRef]
26. Ukraintsev, A.A.; Kutuzov, M.M.; Lavrik, O.I. Studying structure and functions of nucleosomes with atomic force microscopy. *Biochemistry* **2024**, *89*, 674–687. [CrossRef]
27. Lowary, P.T.; Widom, J. New DNA sequence rules for high affinity binding to histone octamer and sequence-directed nucleosome positioning. *J. Mol. Biol.* **1998**, *276*, 19–42. [CrossRef]
28. Rogge, R.A.; Kalashnikova, A.A.; Muthurajan, U.M.; Porter-Goff, M.E.; Luger, K.; Hansen, J.C. Assembly of nucleosomal arrays from recombinant core histones and nucleosome positioning DNA. *J. Vis. Exp.* **2013**, *79*, e50354. [CrossRef]
29. Spakman, D.; King, G.A.; Peterman, E.J.G.; Wuite, G.J.L. Constructing arrays of nucleosome positioning sequences using Gibson Assembly for single-molecule studies. *Sci. Rep.* **2020**, *10*, 9903. [CrossRef]
30. Amé, J.C.; Kalisch, T.; Dantzer, F.; Schreiber, V. Purification of recombinant poly(ADP-ribose) polymerases. *Methods Mol. Biol.* **2011**, *780*, 135–152. [CrossRef]
31. Peterson, C.L.; Hansen, J.C. Chicken erythrocyte histone octamer preparation. *CSH Protoc.* **2008**, *2008*, pdb.prot5112. [CrossRef]
32. Belousova, E.A.; Ishchenko, A.A.; Lavrik, O.I. DNA is a new target of PARP3. *Sci. Rep.* **2018**, *8*, 4176. [CrossRef]
33. Kutuzov, M.M.; Kurgina, T.A.; Belousova, E.A.; Khodyreva, S.N.; Lavrik, O.I. Optimization of nucleosome assembling from histones and model DNAs and estimation of the reconstitution efficiency. *Biopolym. Cell* **2019**, *35*, 91–98. [CrossRef]
34. Pyne, A.L.B.; Hoogenboom, B.W. Imaging DNA structure by atomic force microscopy. *Methods Mol. Biol.* **2016**, *1431*, 47–60. [CrossRef]
35. Xin, Y.; Zargariantabrizi, A.A.; Grundmeier, G.; Keller, A. Magnesium-free immobilization of DNA origami nanostructures at mica surfaces for atomic force microscopy. *Molecules* **2021**, *26*, 4798. [CrossRef]
36. Melters, D.P.; Bui, M.; Rakshit, T.; Grigoryev, S.A.; Sturgill, D.; Dalal, Y. High-resolution analysis of human centromeric chromatin. *Life Sci. Alliance* **2025**, *8*, e202402819. [CrossRef]
37. Billingsley, D.J.; Kirkham, J.; Bonass, W.A.; Thomson, N.H. Atomic force microscopy of DNA at high humidity: Irreversible conformational switching of supercoiled molecules. *Phys. Chem. Chem. Phys.* **2010**, *12*, 14727–14734. [CrossRef]
38. Billingsley, D.J.; Lee, A.J.; Johansson, N.A.; Walton, A.; Stanger, L.; Crampton, N.; Bonass, W.A.; Thomson, N.H. Patchiness of ion-exchanged mica revealed by DNA binding dynamics at short length scales. *Nanotechnology* **2014**, *25*, 025704. [CrossRef]
39. Koshkina, D.; Maluchenko, N.; Nilov, D.; Lyubitelev, A.; Korovina, A.; Pushkarev, S.; Armeev, G.; Kirpichnikov, M.; Studitsky, V.; Feofanov, A. Non-classical H1-like PARP1 binding to chromatosome. *Cells* **2025**, *14*, 1309. [CrossRef]
40. Muthurajan, U.M.; Hepler, M.R.; Hieb, A.R.; Clark, N.J.; Kramer, M.; Yao, T.; Luger, K. Automodification switches PARP-1 function from chromatin architectural protein to histone chaperone. *Proc. Natl. Acad. Sci. USA* **2014**, *111*, 12752–12757. [CrossRef]
41. Bell, N.A.W.; Haynes, P.J.; Brunner, K.; de Oliveira, T.M.; Flocco, M.M.; Hoogenboom, B.W.; Molloy, J.E. Single-molecule measurements reveal that PARP1 condenses DNA by loop stabilization. *Sci. Adv.* **2021**, *7*, eabf3641. [CrossRef]
42. Bell, N.A.W.; Molloy, J.E. Single-molecule force spectroscopy reveals binding and bridging dynamics of PARP1 and PARP2 at DNA double-strand breaks. *Proc. Natl. Acad. Sci. USA* **2023**, *120*, e2214209120. [CrossRef]
43. Chappidi, N.; Quail, T.; Doll, S.; Vogel, L.T.; Aleksandrov, R.; Felekyan, S.; Kühnemuth, R.; Stoynov, S.; Seidel, C.A.M.; Brugués, J.; et al. PARP1-DNA co-condensation drives DNA repair site assembly to prevent disjunction of broken DNA ends. *Cell* **2024**, *187*, 945–961.e18. [CrossRef]
44. Rouleau, M.; McDonald, D.; Gagné, P.; Ouellet, M.E.; Droit, A.; Hunter, J.M.; Dutertre, S.; Prigent, C.; Hendzel, M.J.; Poirier, G.G. PARP-3 associates with polycomb group bodies and with components of the DNA damage repair machinery. *J. Cell. Biochem.* **2007**, *100*, 385–401. [CrossRef]

Disclaimer/Publisher's Note: The statements, opinions and data contained in all publications are solely those of the individual author(s) and contributor(s) and not of MDPI and/or the editor(s). MDPI and/or the editor(s) disclaim responsibility for any injury to people or property resulting from any ideas, methods, instructions or products referred to in the content.